THE IMPORTANCE OF QUADRUPOLE SOURCES IN PREDICTION OF TRANSONIC TIP SPEED PROPELLER NOISE

Donald B. Hanson
Hamilton Standard Division of United Technologies Corporation

Martin R. Fink
United Technologies Research Center

SUMMARY

A theoretical analysis is presented for the harmonic noise of high speed, open rotors. Far field acoustic radiation equations based on the Ffowcs-Williams/Hawkings theory are derived for a static rotor with thin blades and zero lift. Near the plane of rotation, the dominant sources are the volume displacement and the ρu^2 quadrupole, where u is the disturbance velocity component in the direction of blade motion. These sources are compared in both the time domain and the frequency domain using two-dimensional airfoil theories valid in the subsonic, transonic, and supersonic speed ranges. For nonlifting parabolic arc blades, the two sources are equally important at speeds between the section critical Mach number and a Mach number of one. However, for moderately subsonic or fully supersonic flow over thin blade sections, the quadrupole term is negligible. It is therefore concluded for thin blades that significant quadrupole noise radiation is strictly a transonic phenomenon and that it can be suppressed with blade sweep. Noise calculations are presented for two rotors, one simulating a helicopter main rotor and the other a model propeller tested at United Technologies Corporation. For the latter, agreement with test data was substantially improved by including the quadrupole source term.

INTRODUCTION

In the 1970's there has been a renewed interest in noise of open rotors, not only for helicopter application, but because of a development program in the United States for fuel conservative propulsion systems. Ffowcs-Williams and Hawkings provided a theoretical basis (ref. 1) for analyzing this type of problem by showing that, in principle, the noise can be calculated exactly if certain aerodynamic quantities (source

This paper was originally presented at the Spring Meeting of the Institute of Acoustics, Cambridge University, Cambridge, England, April 7, 1978. The manuscript has been submitted for possible publication in the Journal of Sound and Vibration and is reproduced herein by permission of the editor of that journal.

terms) are known on and around the blades. The surface sources are the volume displacement and the blade surface forces. The volume sources are quadrupole terms representing shear stress in the air. The propeller noise problem is an ideal application of the theory because the blades are thin and, in forward flight, the sources are essentially steady in the blade coordinate system.

Because the surface source terms are linear, considerable progress has been made in developing techniques for computing their noise (refs. 2, 3, 4). However, the quadrupoles have been neglected because they are second order in the disturbance velocities, which makes them appear small. This appeared justified because the linear theories worked reasonably well for moderate speed propellers. Also, sonic boom theory, which uses only the linear volume displacement and loading sources, is successful at supersonic aircraft speeds. However, Kitaplioglu and George (ref. 5) remarked in a recent paper that the linear theories consistently underpredict noise from rotors operating at the transonic speeds which are currently of interest. An example of this is the transonic propeller in figure 1 which was run at United Technologies Research Center. Figure 2 shows test versus linear theory from ref. 4. Maximum noise along the fuselage occurs near the plane of rotation, where noise levels predicted from the surface sources are as much as 5 dB lower than the data. After considering other mechanisms, the quadrupole source was investigated as an explanation for this underprediction.

The purpose of this report is to illustrate the role of the quadrupole sources in noise radiation from open rotors using the simplest possible meaningful example. To accomplish this, far field radiation equations are derived for a static, nonlifting rotor. The equations are cast into a form which permits direct comparison of the volume displacement and quadrupole sources inside the radiation integrals. The source terms are then evaluated using aerodynamic techniques which are valid through the subsonic, transonic, and supersonic ranges. Finally, some sample noise calculations are presented.

SYMBOLS

b	airfoil chord
B	number of blades
$B_D \equiv b/D$	chord-to-diameter ratio
c_o	ambient speed of sound
D	propeller diameter
f_i	i^{th} component of force/unit area exerted by airfoil on fluid
G	Green's function (eq. 2)
h	thickness distribution (figure 3)

H	h/b, normalized thickness distribution (figure 4)
i, j	1, 2, 3 Cartesian coordinate indices
J_n	Bessel function
k	specific heat ratio, 1.4 for air
m	harmonic of blade passing frequency
M_r	$\Omega \frac{r_o}{c_o}$, section relative Mach number
M_T	$\Omega \frac{r_T}{c_o}$, tip rotational Mach number
n	mB, harmonic of shaft frequency
p	acoustic pressure
P_n	complex Fourier coefficient of p
P_{Vn}	volume displacement portion of P_n
P_{Qn}	quadrupole portion of P_n
r	distance from origin to observer point
r_o	distance from origin to source point on blade
r_T	propeller tip radius, D/2
R	$\left\vert \vec{x} - \vec{y} \right\vert$, distance from source point to observer
S	source surface in eq. 1
t	observer time
T	integration limit for source time (τ) integration
T_{ij}	$\rho u_i u_j$, quadrupole (shear stress) source
u	component in chordwise direction of disturbance velocity
u_i	component in i^{th} direction of disturbance velocity
U	Ωr_o, local blade section speed
v	component normal to chord of disturbance velocity
V_n	normal component of airfoil surface velocity
$\vec{x}$	(x, y, 0), observer coordinates (figure 3)
X	γ/b, normalized chordwise coordinate
y	observer distance from propeller axis (figure 3)
y_i	source coordinates y_1, y_2, y_3

Y	ξ/b, normalized coordinate perpendicular to chord and to radius
Z	$\frac{r_o}{r_T}$, normalized radial coordinate
ξ	source coordinate normal to chord (figure 3)
γ	source coordinate in chordwise direction (figure 3)
δ	Dirac delta (impulse) function
θ	angle from propeller axis to observer point
ν	source volume (volume exterior to blades)
ρ	density
ρ_o	ambient density
τ	source time variable
Ψ_V	integrated volume displacement source strength in frequency domain (eqs. 31, 34)
Ψ_{ij}	integrated quadrupole strength in frequency domain (eq. 33)
Ψ_{11}	integrated strength of ρu^2 quadrupole in frequency domain
ω	radian frequency of sound
Ω	2π times shaft rotation frequency

$\rightarrow$ indicates vector, as in $\vec{x}$

$'$ indicates differentiation with respect to argument, as in h'

ACOUSTIC THEORY

The starting point for the analysis is Goldstein's version of the acoustic analogy (eq. 3.6, ref. 6) from which the Ffowcs-Williams/Hawkings formulas (ref. 1) can be derived:

$$\rho'(\vec{x},t) = \frac{1}{c_o^2}\int_{-T}^{T}\int_{S(\tau)}\left(-\rho_o V_n \frac{\partial G}{\partial \tau} + f_i \frac{\partial G}{\partial y_i}\right) dS(\vec{y})\, d\tau$$

$$+ \frac{1}{c_o^2}\int_{-T}^{T}\int_{\nu(\tau)} T_{ij} \frac{\partial^2 G}{\partial y_i \partial y_j}\, d\vec{y}\, d\tau \qquad (1)$$

This equation gives the disturbance density ρ' exactly for known values of the source terms. The sources to be evaluated on the moving surface $S(\tau)$ are the normal surface velocity V_n (taken to be positive outward, the opposite of Goldstein's convention) and the surface force components f_i. The quadrupole source is the

Lighthill stress tensor T_{ij} which is to be evaluated in the volume around the blades $\nu(\tau)$. The source time (τ) integration is over a range $-T \leq \tau \leq T$ large enough to include all signals from the source region which arrive at the observation point at time t. G is the Green's function

$$G = \frac{\delta(t-\tau-R/c_o)}{4\pi R} \tag{2}$$

where $R = |\vec{x} - \vec{y}|$ is the distance between source point $\vec{y}$ and observer point $\vec{x}$.

For a thin, nonlifting propeller blade, the surface forces f_i can be neglected. Also, we make the usual approximations that the acoustic pressure

$$p = c_o^2 \rho' \tag{3}$$

where c_o is the ambient sound speed and

$$T_{ij} = \rho u_i u_j \tag{4}$$

where ρ is the density and u_i is the disturbance velocity component in the i^{th} direction. The pressure term in T_{ij} is neglected for now but can be added at any time in the analysis. For the static propeller, we approximate the Cartesian source coordinates with locally orthogonal curvilinear coordinates as shown in figure 3:

$$y_1 = \gamma \qquad y_2 = \xi \qquad y_3 = r_o$$

The observer coordinates are x, y, 0.

The distance R is given by

$$R = \sqrt{(x+\xi)^2 + y^2 + r_o^2 - 2yr_o \cos\left(\frac{\gamma}{r_o}\right)} \tag{6}$$

In the far field Green's function

$$G = \frac{\delta(t-\tau-R/c_o)}{4\pi r} \tag{7}$$

only the terms of order ξ/r and r_o/r in a series expansion of R are retained, giving

$$R \rightarrow r + \xi \cos\theta - r_o \sin\theta \cos\left(\frac{\gamma}{r_o}\right) \tag{8}$$

where θ is the angle of the observer from the propeller axis.

Since the blades of interest are thin, we consider the surface sources to act on the mean chord line $\xi = 0$ and neglect the volume occupied by the blade. This is easily justified, for example, with blades 2% thick and a 0.15 chord-to-diameter ratio operating at a tip Mach number of 1.0 because the maximum error in point of action of the sources is less than the wavelength of the 2000th harmonic of shaft rotation frequency. To evaluate the surface integral at $\tau = 0$, we note that $V_n \, dS = \frac{1}{2} U h'(\gamma) \, d\gamma \, dr_o$ for each surface of the airfoil. Here $U = \Omega r_o$ is the local blade section speed, $h(\gamma)$ is the airfoil thickness distribution shown in figure 3, and the prime on h denotes differentiation with respect to the argument. The only time dependence of the sources considered here is that due to convection at speed U in the negative γ direction, so the source behavior is given simply by $h(\gamma + U\tau)$ and $T_{ij}(\gamma + U\tau)$.

From these arguments, eq. 1 reduces to

$$p(\vec{x}, t) = \int_{-\infty}^{\infty} \int_{0}^{r_T} \int_{-\pi r_o}^{\pi r_o} -\rho_o U h'(\gamma + U\tau) \frac{\partial G}{\partial \tau} \, d\gamma \, dr_o \, d\tau$$
$$+ \int_{-\infty}^{\infty} \int_{0}^{\infty} \int_{-\pi r_o}^{\pi r_o} \int_{-\infty}^{\infty} \left[T_{11}(\gamma + U\tau) \frac{\partial^2 G}{\partial \gamma^2} + 2T_{12}(\gamma + U\tau) \frac{\partial^2 G}{\partial \gamma \partial \xi} + T_{22}(\gamma + U\tau) \frac{\partial^2 G}{\partial \xi^2} \right] d\xi \, d\gamma \, dr_o \, d\tau \tag{9}$$

where the integrations over upper and lower airfoil surfaces are lumped together using γ as an integration parameter and r_T is the blade tip radius. T has been set to ∞, assuming the τ integrals will converge. The sum on i and j has been performed neglecting any radial velocity disturbances so that the remaining quadrupole sources are

$$T_{11} = \rho u^2 \tag{10}$$

$$T_{12} = \rho u v \tag{11}$$

$$T_{22} = \rho v^2 \tag{12}$$

where u and v are as shown in figure 3. The great simplification brought to eq. 9 by the thin blade approximation is that the γ and ξ integration limits no longer depend on τ. Thus, the integrations may be performed in any order. Equation 9 gives the noise caused by one blade; the other blades are accounted for by superposition.

The derivatives of the Green's function with respect to τ and γ are shifted temporarily onto the source functions using integration by parts.

$$p(\vec{x}, t) = \int_{-\infty}^{\infty}\int_{0}^{r_T}\int_{-\pi r_o}^{\pi r_o} \rho_o U^2 h''(\gamma + U\tau)\, G\, d\gamma\, dr_o\, d\tau$$

$$+ \int_{-\infty}^{\infty}\int_{0}^{\infty}\int_{-\pi r_o}^{\pi r_o}\int_{-\infty}^{\infty} \left[T_{11}''(\gamma + U\tau)\, G - 2\, T_{12}'(\gamma + U\tau)\, \frac{\partial G}{\partial \xi} + T_{22}(\gamma + U\tau)\, \frac{\partial^2 G}{\partial \xi^2}\right] d\xi\, d\gamma\, dr_o\, d\tau \tag{13}$$

Because h' is discontinuous at the blade leading and trailing edges and because the T_{ij}'s are discontinuous across shocks, their derivatives must, at this point, be considered as generalized functions in the sense described by Farassat (ref. 7). The differentiations will shortly be removed from the sources. The derivatives $\frac{\partial G}{\partial \xi}$ and $\frac{\partial^2 G}{\partial \xi^2}$ can be evaluated explicitly from eqs. 7 and 8:

$$\frac{\partial G}{\partial \xi} = -\frac{\cos\theta}{4\pi c_o r}\, \delta'(t - \tau - R/c_o) \tag{14}$$

$$\frac{\partial^2 G}{\partial \xi^2} = \frac{\cos^2\theta}{4\pi c_o^2 r}\, \delta''(t - \tau - R/c_o) \tag{15}$$

Substitution of these into eq. 13 eliminates derivatives with respect to ξ. The derivatives with respect to the argument of the delta function can be removed using integration by parts on the τ integral.

$$p(\vec{x}, t) = \frac{1}{4\pi r}\int_{-\infty}^{\infty}\int_{0}^{r_T}\int_{-\pi r_o}^{\pi r_o} \rho_o U^2 h''(\gamma + U\tau)\, \delta(t - \tau - R/c_o)\, d\gamma\, dr_o\, d\tau$$

$$+ \frac{1}{4\pi r}\int_{-\infty}^{\infty}\int_{0}^{\infty}\int_{-\pi r_o}^{\pi r_o}\int_{-\infty}^{\infty} \left[T_{11}''(\gamma + U\tau) + 2\,\frac{U\cos\theta}{c_o}\, T_{12}''(\gamma + U\tau) + \frac{U^2\cos^2\theta}{c_o^2}\, T_{22}''(\gamma + U\tau)\right] \delta(t - \tau - R/c_o)\, d\xi\, d\gamma\, dr_o\, d\tau \tag{16}$$

Time Domain Radiation Equations

The τ integration is now trivial, simply replacing the arguments $\gamma + U\tau$ by $\gamma + Ut - M_r R$ where $M_r = U/c = \Omega r_o/c_o$ is the section relative Mach number.

$$p(\vec{x}, t) = \frac{1}{4\pi r}\int_{0}^{r_T}\int_{-\pi r_o}^{\pi r_o} \rho_o U^2 h''(\gamma + Ut - M_r R)\, d\gamma\, dr_o$$

$$+ \frac{1}{4\pi r}\int_{0}^{\infty}\int_{-\pi r_o}^{\pi r_o}\int_{-\infty}^{\infty} \left[T_{11}''(\gamma + Ut - M_r R) + 2\, M_r \cos\theta\, T_{12}''(\gamma + Ut - M_r R) + M_r^2 \cos^2\theta\, T_{22}''(\gamma + Ut - M_r R)\right] d\xi\, d\gamma\, dr_o \tag{17}$$

The derivatives are removed from the source functions by noting that $\frac{\partial^2}{\partial t^2} h(\gamma + Ut - M_r R) = U^2 h''(\gamma + Ut - M_r R)$ and that $\frac{\partial^2}{\partial t^2}$ can be moved outside the integrals because the limits are independent of t.

$$p(\vec{x}, t) = \frac{1}{4\pi r} \frac{\partial^2}{\partial t^2} \int_0^{r_T} \int_{-\pi r_o}^{\pi r_o} \rho_o h (\gamma + Ut - M_r R) \, d\gamma \, dr_o$$

$$+ \frac{1}{4\pi r} \frac{\partial^2}{\partial t^2} \int_0^{\infty} \int_{-\pi r_o}^{\pi r_o} \int_{-\infty}^{\infty} \frac{1}{U^2} T_{11} (\gamma + Ut - M_r R) + 2 \frac{\cos\theta}{U c_o} T_{12} (\gamma + Ut - M_r R) + \frac{\cos^2\theta}{c_o^2} T_{22} (\gamma + Ut - M_r R) \quad d\xi \, d\gamma \, dr_o \tag{18}$$

The γ integrations in eqs. 17 and 18 run from $-\pi r_o$ to πr_o. However, $h(\gamma + Ut - M_r R)$ is zero except for values of γ satisfying

$$2\pi N r_o - \frac{b}{2} < \gamma + Ut - M_r R < 2\pi N r_o + \frac{b}{2} \tag{19}$$

where N is an integer. Finding these values of γ is equivalent to finding the acoustic planform or retarded blade location as described in ref. 4.

The first integral in eq. 18 is the traditional thickness noise which is the direct result of volume displacement at the surface of the blade. This surface integral over the rotor disc was derived previously by Hanson (ref. 4) and was shown to give the same result as Farassat's theory (ref. 2). The second integral in eq. 18 is the quadrupole thickness noise which is also a result of volume displacement but is accounted for by integrating the associated stress terms T_{11}, T_{12}, and T_{22} over the volume surrounding the rotor disc. The quadrupole term has not been calculated correctly in previous work.

Equation 18 has been presented in a form which shows that the T_{11} quadrupole (integrated over ξ) radiates exactly like the volume displacement source with regard to frequency and directivity dependence. Since T_{12} and T_{22} are multiplied by $\cos\theta$, we need only compare chordwise distributions of

$$\frac{h}{b} \quad \text{versus} \quad \int_{-\infty}^{\infty} \frac{\rho u^2}{\rho_o U^2} \, d\left(\frac{\xi}{b}\right) \tag{20}$$

to compare contributions of the two sources to noise near the plane of rotation. This is done in a later section entitled "Aerodynamic Evaluation of Quadrupole Source Term."

The time domain equations can be transformed to blade fixed coordinates by substituting $\eta = \gamma + Ut - M_r R$. Since this might be an advantage for subsonic tip speed rotors, an example is given in the appendix.

Frequency Domain Radiation Equations

It is also useful to compare these sources in the frequency domain, which is done by calculating complex Fourier coefficients from either eq. 17 or eq. 18 according to

$$P_n(\vec{x}) = \frac{\Omega}{2\pi}\int_0^{2\pi/\Omega} p(\vec{x}, t)\, e^{in\Omega t}\, dt \tag{21}$$

The volume displacement term from eq. 18 becomes

$$P_{Vn}(\vec{x}) = -\frac{\rho_o n^2 \Omega^2}{4\pi r}\int_0^{r_T}\int_{-\pi r_o}^{\pi r_o}\frac{\Omega}{2\pi}\int_0^{\frac{2\pi}{\Omega}} h(\gamma + Ut - M_r R)\, e^{in\Omega t}\, dt\, d\gamma\, dr_o \tag{22}$$

where the factor $-n^2\Omega^2$ in the frequency domain comes from $\frac{\partial^2}{\partial t^2}$ in the time domain.

We change variables with

$$Xb = \gamma + Ut - M_r R \tag{23}$$

Then, because the surface source is assumed to act on the mean chordline $\xi = 0$, eq. 8 gives

$$t = \frac{Xb}{\Omega r_o} - \frac{\gamma}{\Omega r_o} + \frac{r}{c_o} - \frac{r_o}{c_o}\sin\theta\, \cos\left(\frac{\gamma}{r_o}\right) \tag{24}$$

This results in

$$P_{Vn}(\vec{x}) = -\frac{\rho_o n^2 \Omega^2}{4\pi r}\, e^{in\frac{\Omega r}{c_o}}\int_0^{r_T} b\left[\int_{-\frac{1}{2}}^{\frac{1}{2}} h(Xb)\, e^{in\frac{bX}{r_o}}\, dX \cdot \frac{1}{2\pi r_o}\int_0^{2\pi r_o} e^{-in\frac{\gamma}{r_o} - in\frac{\Omega r_o}{c_o}\sin\theta\, \cos\frac{\gamma}{r_o}}\, d\gamma\right] dr_o \tag{25}$$

The γ integration gives Bessel functions so that eq. 25 reduces to

$$P_{Vn}(\vec{x}) = -\frac{\rho_o n^2 \Omega^2}{4\pi r}\, e^{in\left(\frac{\Omega r}{c_o} - \frac{\pi}{2}\right)}\int_0^{r_T} J_n\left(\frac{n\Omega r_o}{c_o}\sin\theta\right) b\int_{-\frac{1}{2}}^{\frac{1}{2}} h(bX)\, e^{i\frac{nb}{r_o}X}\, dX\, dr_o \tag{26}$$

which is the same result derived by Hawkings and Lowson (ref. 3). Equation 26 is now normalized using

$$Z = \frac{r_o}{r_T} \tag{27}$$

$$M_T = \frac{\Omega r_T}{c_o} \tag{28}$$

$$B_D = \frac{b}{D} \tag{29}$$

and the thickness function $H(X) = h(bX)/b$ shown in figure 4 to arrive at the final form for the volume displacement noise component:

$$P_{Vn}(\vec{x}) = -\rho_o c_o^2 \frac{n^2 M_T^2}{\pi\left(\frac{r}{r_T}\right)} e^{in\left(\frac{\Omega r}{c_o} - \frac{\pi}{2}\right)} \int_0^1 B_D^2 J_n(nZ M_T \sin\theta) \psi_V\left(\frac{2nB_D}{Z}\right) dZ \tag{30}$$

where

$$\psi_V\left(\frac{2nB_D}{Z}\right) = \int_{-\frac{1}{2}}^{\frac{1}{2}} H(X) e^{i\frac{2nB_D}{Z}X} dX \tag{31}$$

is the Fourier transform of the airfoil thickness distribution. The same manipulations for the quadrupole term in eq. 18 give

$$P_{Qn}(\vec{x}) = -\rho_o c_o^2 \frac{n^2 M_T^2}{\pi\left(\frac{r}{r_T}\right)} e^{in\left(\frac{\Omega r}{c_o} - \frac{\pi}{2}\right)} \int_0^\infty B_D^2 J_n(nZ M_T \sin\theta) \times (\psi_{11} + 2Z M_T \cos\theta \psi_{12} + Z^2 M_T^2 \cos^2\theta \psi_{22}) dZ \tag{32}$$

where $Y = \xi/b$ and

$$\psi_{ij}\left(\frac{2nB_D}{Z}\right) = \int_{-X_1}^{X_1} \int_{-\infty}^{\infty} \frac{\rho u_i u_j}{\rho_o U^2} e^{2in B_D M_T \cos\theta Y} dY e^{i\frac{2nB_D}{Z}X} dX \tag{33}$$

is the integrated quadrupole source term. The chordwise integration is over a range $\pm X_1$ equivalent to $\pm \Omega r_o$. Because eqs. 30 and 32 are in the same form, the two sources can be compared in the frequency domain by comparing the source terms ψ_V and ψ_{11}. This and the time domain comparison are the subjects of the following section.

AERODYNAMIC EVALUATION OF QUADRUPOLE SOURCE TERM

It is well known from experimental studies that noise of high speed rotors is maximum near the plane of rotation. Since $\cos\theta = 0$ in the plane of rotation, the preceding acoustic analysis shows that the volume displacement and quadrupole thickness sources can be compared by calculating

$$\Psi_V = \int_{-\frac{1}{2}}^{\frac{1}{2}} H(X)\, e^{i\frac{2m\,B\,B_D}{Z}X}\, dX \tag{34}$$

and

$$\Psi_{11} = \int_{-\infty}^{\infty}\int_{-\infty}^{\infty} \frac{\rho\, u^2}{\rho_\infty U^2}\, e^{i\frac{2m\,B\,B_D}{Z}X}\, dY\, dX \tag{35}$$

where n has been replaced by mB and m is the harmonic of blade passing frequency. The streamwise velocity perturbation is u and ρ is the local density. The chordwire integration is shown with an infinite range because the source is now considered to be "unwrapped" to allow use of two dimensional airfoil theory for evaluation by Ψ_{11}. These source terms have been evaluated for biconvex parabolic airfoils,

$$H(X) = (1 - 4X^2)\,\frac{h_{max}}{b} \tag{36}$$

and the results are presented below.

Aerodynamic Theory

The airfoil flow field was studied using different computation schemes for fully subsonic, transonic, and fully supersonic flow as described herein. All calculations were two dimensional and assumed small disturbances so that the density ratio could be calculated from the small perturbation approximation for isentropic compressible flow

$$\frac{\rho}{\rho_\infty} = \left\{1 - \frac{k-1}{2} M_r^2 \left[\frac{(U+u)^2 + v^2}{U^2} - 1\right]\right\}^{\frac{1}{k-1}} \approx 1 - M_r^2\,\frac{u}{U} \tag{37}$$

where k is the ratio of specific heats.

For fully subsonic flow, velocity distributions were calculated using the Spreiter and Alksne local linearization method as given in ref. 8.

For fully supersonic flow, explicit first order solutions for the supersonic flow field of a parabolic arc airfoil were taken from Caughey (ref. 9). The calculated shock wave positions for a 2% thickness ratio airfoil at a Mach number of 1.15 are plotted in figure 5. Because of the spreading shock waves, the quadrupole noise originates from an increasingly noncompact region at increasing heights above the airfoil. Streamwise perturbation velocities near the surface are predicted to vary inversely as $\sqrt{M_r^2 - 1}$, as is also predicted by linearized supersonic theory. Thus, the ratio of quadrupole to volume displacement acoustic pressure is predicted to increase as supersonic Mach number is decreased and the largest value of this ratio should occur in the transonic regime.

For transonic flow, elaborate digital computer programs are available for detailed calculation of transonic flow past two-dimensional airfoils. Rather than modify one of those programs to calculate the spatial distribution of perturbation velocity, an older approximate method for transonic flow was modified by use of information available from the newer, more rigorous solutions. This modified solution is also based on the local linearization method developed by Spreiter and Alksne (ref. 8). In that method, the streamwise velocity gradient in a locally subsonic portion of the flow field is obtained from its value for incompressible flow by

$$\frac{d}{dX}\left(\frac{u}{U}\right) = \left[1 - M_r^2 - (k+1)\, M_r^2\, \frac{u}{U}\right]^{-\frac{1}{2}} \frac{d}{dX}\left(\frac{u}{U}\right)_{M_r = 0} \tag{38}$$

Here, the quantity in square brackets is one minus the local axial component of Mach number squared. Similarly, streamwise velocity gradient in a locally supersonic flow field is obtained from its value as calculated from linearized supersonic theory at a free stream Mach number $\sqrt{2}$ by

$$\frac{d}{dX}\left(\frac{u}{U}\right) = \left[M_r^2 - 1 + (k+1)\, M_r^2\, \frac{u}{U}\right]^{-\frac{1}{2}} \frac{d}{dX}\left(\frac{u}{U}\right)_{M_r = \sqrt{2}} \tag{39}$$

Also, streamwise velocity gradient in an accelerating near-sonic flow was shown to be equal to its value at the same location at a free stream Mach number of one, divided by free stream Mach number to the 2/3 power.

Equations were given by Spreiter and Alksne in ref. 8 for calculating the streamwise perturbation velocity within these three regions, assuming that the value of this velocity was known at one chordwise position. This velocity, and therefore the constant of integration when integrating the above velocity derivatives, was known only for

the cases of fully subsonic, near sonic, and fully supersonic flow. Fortunately, numerical solutions for the flow field of a nonlifting parabolic arc airfoil are available for transonic Mach numbers less than one (Murman and Cole, ref. 10) and greater than one (Murman, ref. 11). These numerical results can be utilized to evaluate the variations of any flow property of interest throughout the transonic range. In particular, it had been noted in ref. 8 that the equation for perturbation velocity in accelerating near-sonic flow had a denominator that went to zero at the sonic point on the airfoil surface. To obtain valid results, the numerator also had to go to zero such that their ratio remained locally constant. The analytical solutions for fully subsonic flow, fully supersonic flow, and free stream Mach numbers very near one and the numerical results in refs. 10 and 11 for the intermediate regions were utilized to prescribe the streamwise perturbation velocity at this chordwise position (for a parabolic arc airfoil, the quarter-chord).

Velocity gradients calculated from eqs. 38 and 39 should be reasonably accurate if the local Mach number is not near one. As local Mach number approaches one, the calculated gradients approach infinity. Therefore if one starts with a prescribed locally subsonic velocity at some chordwise location and numerically integrates eq. 41 in the downstream (increasing local velocity) direction, incorrect results would be obtained at nearly sonic local Mach numbers. As with the calculation method described by Fink (ref. 12) for axisymmetric transonic flow, the numerical integration has been modified to use velocity gradients calculated for accelerating near-sonic flow at the chordwise position where it gives a smaller gradient. Further downstream where the flow was locally supersonic, the velocity gradients calculated for accelerating transonic flow and for locally supersonic flow were compared, and the smaller value was used in numerical integration.

Shock wave position was prescribed by use of a curve fitted to the positions given in ref. 10 for this airfoil section. Shock wave strength in the presence of a boundary layer was obtained by an approximation to the data correlation given by Sinnott in ref. 13. The variation of perturbation velocity with distance above and below the airfoil was calculated from the Spreiter and Alksne theory (eqs. 63 and 64 of ref. 14) for positive perturbation velocities and by

$$\frac{u}{U} = \left(\frac{u}{U}\right)_{\xi = 0} \left(1 + \left|\frac{\xi}{h_{max}}\right|\right)^{-1} \tag{40}$$

for negative perturbation velocities at subsonic free stream Mach numbers.

To check the validity of this transonic theory, comparisons have been made with calculations from the exact theory of Carlson using the TRANDES computer program (ref. 15). Mach number distributions around the blade matched well enough to justify use of the approximate theory, which requires two orders of magnitude less computer time.

Calculated Aerodynamic Flow Field

Variations of streamwise perturbation velocity along the chord, as calculated for transonic Mach numbers from 0.80 to 1.04 and also for Mach numbers of 0 to 1.15, are plotted in figure 6 for a 2% thickness ratio parabolic arc airfoil. As Mach number was increased from 0 to 0.8, calculated perturbation velocities increased by approximately a factor of $\left(1-M_r^2\right)^{-\frac{1}{2}}$ as would have been predicted by linearized subsonic theory. Further increase to 0.90 caused a relatively larger increase of maximum perturbation velocity so that the velocity distribution was relatively more peaked than that for incompressible flow. This change in shape of the velocity distribution agrees with that expected for the nonlinear effect of subsonic Mach number as calculated by the Karman-Tsien compressibility correction.

Small increases of Mach number above 0.90 caused the development of locally supersonic flow followed by a shock wave. Calculated values of local velocity ratio upstream of midchord were approximately independent of free stream Mach number in the range from about 0.91 to 0.94. This range of Mach number was characterized by the change from a broad maximum of perturbation velocity near midchord to an accelerating transonic flow with large perturbation velocities.

As free stream Mach number was further increased, a general reduction in perturbation velocity ratio occurred. However, the shock wave continued to move downstream until it reached the trailing edge at a free stream Mach number of about 0.97. The calculated distribution of perturbation velocity for a Mach number of 1.04 resembles that for fully supersonic flow at a Mach number of 1.15 except for having a logarithmic singularity rather than a finite value at the leading edge. This difference corresponds to the presence of a detached shock wave and leading edge stagnation point at 1.04 but an attached shock wave at the sharp leading edge for the higher Mach number.

These velocity distributions and the corresponding densities from eq. 37 were used to calculate the normalized quadrupole strength $\rho u^2/\rho_o U^2$ on the airfoil surface as shown in figure 7. In fully subsonic flow the source distribution for this airfoil is symmetric about midchord with sharp peaks at the leading and trailing edges and a broad peak near midchord. Increasing the free stream Mach number increases the amplitude of this broad peak. Further increase above the critical Mach number causes the growth of a large, strong quadrupole noise-radiating region along the aft 2/3 of the chord. As free stream Mach number is increased through one, the acoustic strength of this aft region decreases and the sharp peak near the leading edge strengthens. Finally, at supersonic Mach numbers large enough to maintain an attached leading edge shock wave, the source strength is concentrated near the leading and trailing edges. The integration of the quadrupole source in the vertical direction is described below; however, if the effective extent of the source above the surface were temporarily assumed to be 1 chord, then the curves in figure 7 would represent $\int (\rho u^2/\rho_o U^2)\, dY$.

This permits the shape and general level of these chordwise quadrupole distributions to be compared with those of the one-sided volume displacement source distribution $H(X)/2$, also plotted in the figure. For subcritical Mach numbers the two distributions are similar. This may explain observations by Schmitz and Yu (ref. 16) and others that the linear theories predict waveshapes like the test data but with levels too low. At supercritical speeds, the downstream shift of the quadrupole will result in a substantially different noise waveform.

Figure 8 shows the vertical distribution of the quadrupole source Ψ_{11} for a combination of B_D, Z, and mB of interest for advanced turbopropeller applications. The ordinate,

$$\frac{1}{\Psi_{11}} \int \frac{\rho u^2}{\rho_\infty U^2} e^{i \frac{2m B B_D}{Z} X} dX \tag{41}$$

is normalized such that each curve has unit area. It can be seen that the quadrupole source extends farther from the airfoil at a Mach number of 0.95 than at 0.90 or 1.00. This, coupled with the trends in $\rho u^2/\rho_\infty U^2$ on the surface as shown in figure 7, leads to a strong peaking of the integrated quadrupole source Ψ_{11} at transonic speeds as shown below.

Figure 8 shows that the effective vertical extent of the quadrupole is about one chord. This means that the two-dimensional aerodynamic theory is probably adequate except near blade tips. It also means that for out of plane noise calculations, noncompactness in the Y direction has to be accounted for with the Y exponential in eq. 33.

Comparison of Volume Displacement and Quadrupole Source Terms

The aerodynamic methods described above are now used to compare the integrated quadrupole source Ψ_{11} with the integrated volume displacement source Ψ_V as functions of radius (i.e., as functions of section relative Mach number, which varies as radius). For the biconvex parabolic airfoil, eqs. 34 and 36 can be integrated analytically to give

$$\Psi_V(\omega_c) = \left[\frac{16}{\omega_c^3} \sin\left(\frac{\omega_c}{2}\right) - \frac{8}{\omega_c^2} \cos\left(\frac{\omega_c}{2}\right) \right] \frac{h_{max}}{b} \tag{42}$$

which is plotted in figure 9. The frequency parameter

$$\omega_c = \frac{2 m B B_D}{Z} \tag{43}$$

is a measure of noncompactness. In the limit as $B_D \to 0$, $\Psi_V \to \frac{2}{3}\frac{h_{max}}{b}$ which (multiplied by b^2) is just the cross-sectional area of the airfoil. The effect of increasing the harmonic order, or increasing the chord at constant section area, is to reduce the noise via chordwise phase interference. The example chosen here for comparison with the quadrupole is the advanced turboprop mentioned above with $B_D = 0.14$ and $B = 8$. For the blade passing frequency fundamental ($m = 1$), figure 9 gives $\Psi_V(2.24) = 0.587\ h_{max}/b$, which is only slightly reduced due to noncompactness.

The quadrupole source was integrated numerically in the X direction from leading edge to trailing edge for the subsonic and transonic cases and from the bow shock to trailing shock for the supersonic case. Integrations in the Y direction were carried out to 20 chords, which figure 8 shows to be well within 1% of the total. The calculated ratios of Ψ_{11} to Ψ_V for a 2% thickness ratio airfoil section are plotted versus section relative Mach number in figure 10 for the 3 speed ranges. The fully subsonic calculations and the transonic calculations are shown to blend well in their range of overlap. The transonic calculations show a peak at $M_r = 0.95$ and then start to decay with increasing Mach number. The increase in calculated values of Ψ_{11} starting at $M_r = 1.05$ is caused by the incorrect assumption that velocity perturbations decay along vertical lines rather than along Mach waves, so that phase cancellation is not correctly represented. The fully supersonic calculations are also shown to diverge at Mach numbers below about 1.15 because the leading edge shock would not be attached as assumed in the theory. Thus, the transonic and supersonic calculations are faired together as shown by the dashed line in figure 10.

The faired curve from figure 10 is replotted in figure 11 as $20 \log_{10} \left| \frac{\Psi_{11} + \Psi_V}{\Psi_V} \right|$ which is the number of decibels added to the volume displacement thickness source by the quadrupole thickness source. Two features are immediately apparent. First, the peak value of 5.7 dB shows clearly that quadrupole radiation is an important factor in high speed rotor noise. Second, the quadrupole source is important only at or very near transonic section speeds. The acoustic results in figure 11 correspond to the well known aerodynamic results from thin airfoil theory in which linear sources and doublets give good performance predictions except near a Mach number of one. It also shows in a unified way why the linear source terms have been adequate for prediction of rotor noise at subcritical tip speeds, why linear source terms are adequate for sonic boom calculations ($M_r > 1.5$), and why linear source models fail for the transonic speeds of interest for advanced propellers and helicopter rotors.

Now that quadrupole noise is recognized as a transonic flow phenomenon, one can ask how to suppress it. Sweep in wings is known to decrease adverse effects of transonic flow if the effective Mach number (product of the relative Mach number and the cosine of the sweep angle) is less than the section critical Mach number. These favorable effects of sweep have also been shown (ref. 17) to occur for rotating blades. Thus, by analogy figure 11 shows for 2% thickness ratio propeller sections, that the additional noise due to the ρu^2 quadrupole should be reduced to less than 1 dB by sweeping the blade to obtain an effective Mach number of 0.85.

ROTOR NOISE CALCULATIONS

In the preceding section, volume displacement and quadrupole sources were compared at relative Mach numbers corresponding to various radii on a blade. It remains to integrate these sources over the blade radius to find the net effect of the quadrupole on radiated noise. This section presents noise calculations for two rotors. The first is a model propeller for which transonic tip speed test data are available and the second is a rectangular planform helicopter rotor previously studied by Farassat (ref. 2).

Transonic Propeller

Figure 2 compared near field data from a transonic tip speed propeller with noise predicted using Hanson's near field theory (ref. 4) for volume displacement and dipole noise surface sources. These data and predictions are replotted in figure 12 along with the noise predicted using a near field version of the present theory for the ρu^2 quadrupole added to the other sources. Including the quadrupole substantially improves the agreement with test data, particularly in, and forward of, the plane of rotation. The remaining underprediction is probably caused by omission of lift effects. Lift is expected to increase the ρu^2 quadrupole and will be the major contributor to the ρuv quadrupole, which can be shown to radiate with the same directivity as the lift dipole. These effects are now being evaluated at United Technologies.

Farassat Rotor

In ref. 2 Farassat predicted thickness noise for a rectangular planform helicopter rotor with 10% thickness ratio parabolic arc blades and a 4% chord-to-diameter ratio. In ref. 4, Hanson showed that the volume displacement term from eq. 18 gave results equivalent to those of Farassat. Figure 13 shows the radial distribution of the additional source strength due to the ρu^2 quadrupole for a tip rotational Mach number of 1.1. As in figure 11, the ordinate is $20 \log_{10} \left|(\Psi_{11} + \Psi_V)/\Psi_V\right|$. For this thick blade, the peak occurs at a lower section speed ($M_r = 0.88$) as would be expected because of the reduced critical Mach number. However, the peak increase of 6.2 dB is nearly the same as for the thinner airfoil (as well as intermediate thicknesses). Since this result was a surprise, it was verified by using an exact inviscid-flow transonic airfoil computer program (ref. 15). It was found that, while the surface values of the quadrupole grow roughly as $(h_{max}/b)^{3/2}$ as predicted by transonic similarity laws, the decay rate with vertical distance increases roughly as $(h_{max}/b)^{\frac{1}{2}}$. The net effect is that the peak value of the quadrupole source Ψ_{11} grows approximately as (h_{max}/b), like the surface source. However, as can be seen by comparing figures 11 and 13, the quadrupole is significant compared to the volume displacement over a wider range of relative Mach numbers for the thicker airfoil.

The effect of the quadrupole integrated over the full radius of the Farassat blade has been checked with eq. 32. For the first several harmonics the noise increase is 3.8 to 4.0 dB in the plane of rotation. However, many more harmonics would have to

be evaluated to find the overall effect on the waveform because of the impulsive nature of the sound from this blade.

CONCLUSIONS

An analysis has been presented for the far field harmonic thickness noise of a nonlifting rotor. The acoustic radiation equations are essentially exact except for the thin blade approximation. The ρu^2 quadrupole has been evaluated using two-dimensional aerodynamic theory valid through the transonic speed range. Comparison of this quadrupole with the volume displacement sources has led to the following conclusions.

1. The ρu^2 quadrupole is an important thickness noise source at transonic blade section speeds. For any thickness ratio, the maximum contribution is roughly 6 dB above the volume displacement thickness noise.

2. For thin propeller blades the quadrupole becomes negligible outside the transonic speed range, which explains why linear source acoustic theories are successful for subcritical propellers and for sonic boom calculations.

3. As thickness ratio is increased, the quadrupole contributes significantly in the range of transonic section speeds found in current helicopter designs.

4. The comparison of theory with test data for a transonic tip speed propeller was substantially improved by adding the ρu^2 quadrupole to the linear source terms.

5. Quadrupole radiation should be reduced to the negligible point if the blades are swept so that their effective Mach number is subcritical.

APPENDIX

Blade-Fixed Coordinates for Time Domain Calculations

As was explained in ref. 4, the time domain equations can be transformed to blade-fixed coordinates by substituting

$$\eta = \gamma + Ut - M_r R \tag{44}$$

For example, the ρu^2 quadrupole pressure from eq. 17 can be written

$$p_{11}(\vec{x}, t) = \frac{1}{4\pi r} \frac{\partial}{\partial t} \iiint \frac{1}{U} T'_{11} (\gamma + Ut - M_r R) \, d\xi \, d\gamma \, dr_o \tag{45}$$

Differentiation of eq. 44 gives

$$d\eta = d\gamma - M_r \frac{\partial R}{\partial \gamma} d\gamma \tag{46}$$

But $M_r \frac{\partial R}{\partial \gamma} = M_{or}$ is the Mach number of the source relative to the observer so that $d\gamma$ can be expressed $d\gamma = d\eta / \left|1 - M_{or}\right|$. Substitution into eq. 45 gives

$$p_{11}(\vec{x}, t) = \frac{1}{4\pi r} \frac{\partial}{\partial t} \int \frac{1}{U} \left[\frac{\frac{\partial}{\partial \eta} (\rho u^2)}{\left|1 - M_{or}\right|} \right]_{ret} d(vol) \tag{47}$$

where $d(vol) = d\xi \, d\eta \, dr_o$. Equation 47 would be practical for numerical computation for subcritical rotors where $1 - M_{or}$ never goes to zero and there are no shock waves to cause discontinuities in ρu^2.

REFERENCES

1. J. E. Ffowcs-Williams and D. L. Hawkings, "Sound Generated by Turbulence and Surfaces in Arbitrary Motion," Philosophical Transaction of the Royal Society of London, Series A, Vol. 264, 1969.

2. F. Farassat, "Theory of Noise Generation from Moving Helicopter Blades with an Application to Helicopter Rotors," NASA TR-R-451, National Aeronautics and Space Administration, Washington, D.C. 1975.

3. D. L. Hawkings and M. V. Lowson, "Theory of Open Supersonic Rotor Noise," J. Sound and Vibration, Vol. 36, No. 1, 1974.

4. D. B. Hanson, "Near Field Noise of High Tip Speed Propellers in Forward Flight," AIAA Paper No. 76-565, 1976.

5. C. Kitaplioglu and A. R. George, "A Study of the Far Field Sound Due to Unsteady Shocks on Rotors," AIAA Paper No. 77-1360, 1977.

6. M. Goldstein, Aeroacoustics, McGraw-Hill, New York, 1976.

7. F. Farassat, "Discontinuities in Aerodynamics and Aeroacoustics, the Concept and Application of Generalized Derivatives," Journal Sound and Vibration, Vol. 55, No. 2, 1977.

8. J. R. Spreiter and A. Y. Alksne, "Thin Airfoil Theory Based on Approximate Solution of the Transonic Flow Equation," NACA Report 1359, 1958.

9. D. A. Caughey, "Second-Order Wave Structure in Supersonic Flows," NASA CR-1438, September 1969.

10. E. M. Murman and J. D. Cole, "Calculation of Plane Steady Transonic Flows," AIAA Journal, Vol. 9, No. 1, January 1971, pp. 114-121.

11. E. M. Murman, "A Relaxation Method for Calculating Transonic Flows With Detached Bow Shocks," Presented at the Third International Conference on Numerical Methods in Fluid Dynamics, Paris, France, July 3-7, 1972.

12. M. R. Fink, "Calculated Transonic Flow Past Slender Fuselages and Afterbodies," Journal of Aircraft, Vol. 8, No. 9, September 1971, pp. 710-716.

13. C. S. Sinnott, "On the Prediction of Mixed Subsonic/Supersonic Pressure Distributions," Journal of the Aerospace Sciences, Vol, 27, No. 10, October 1960, pp. 767-778.

14. J. R. Spreiter and A. Y. Alksne, "Theoretical Prediction of Pressure Distributions on Nonlifting Airfoils at High Subsonic Speeds," NACA Report 1217, 1955.

15. L. A. Carlson, "TRANDES: A Fortran Program for Transonic Airfoil Analysis or Design," NASA CR-2821, June 1977.

16. F. H. Schmitz and Y. H. Yu, "Theoretical Modeling of High Speed Helicopter Impulsive Noise," Paper presented at the Third European Rotorcraft and Powered Lift Aircraft Forum," Aix-en-Provence, France, September 7-9, 1977.

17. W. F. Ballhaus and F. X. Caradonna, "The Effect of Planform Shape on Transonic Flow Past Rotor Tips," AGARD Proceedings #111, Aerodynamics of Rotary Wings. Feb. 1973.

18. R. K. Amiet, "Refraction of Sound by a Shear Layer," AIAA Paper No. 77-54, January 1977.

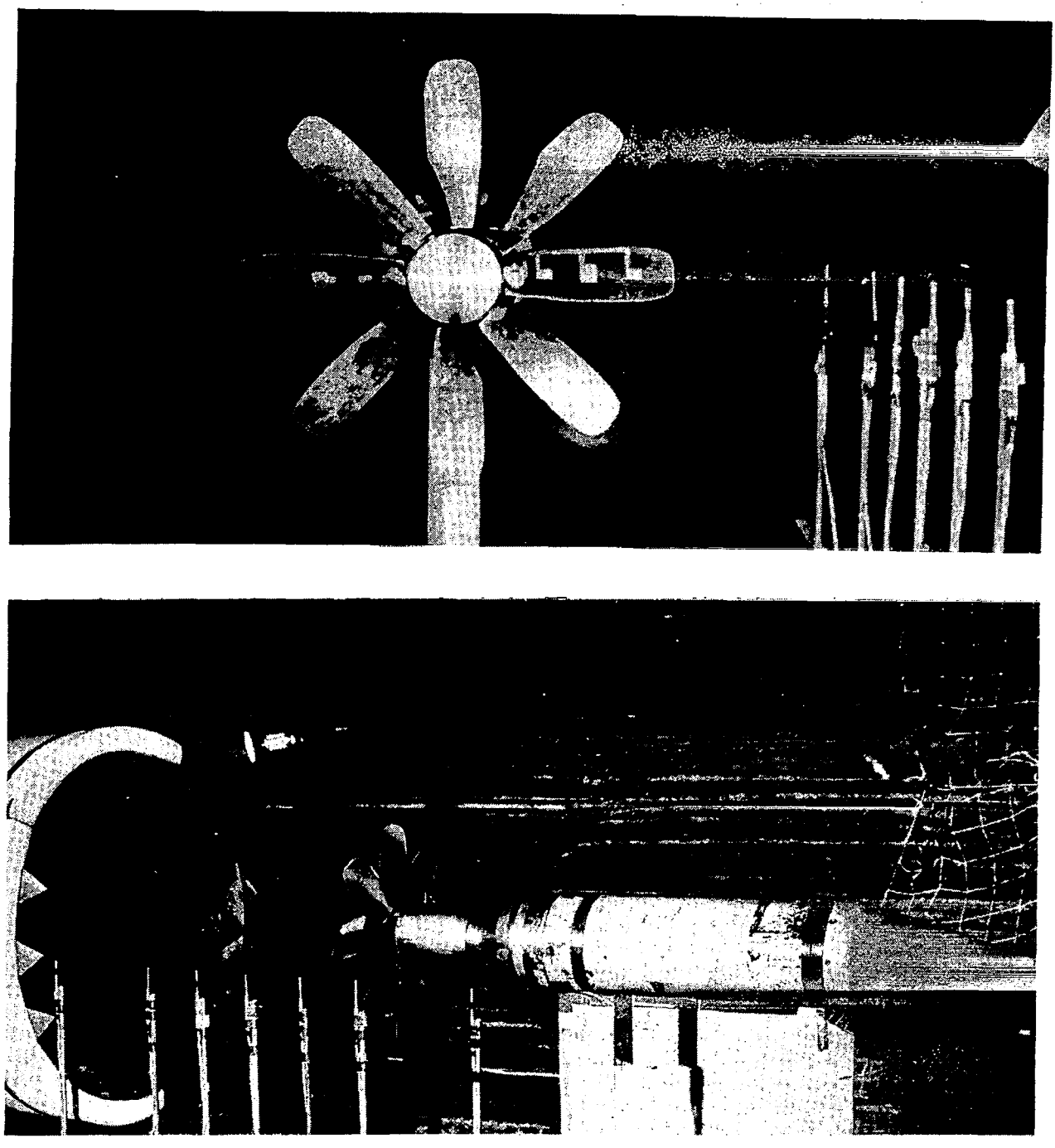

Figure 1.- Transonic tip speed propeller tested in United Technologies Research Center Acoustic Wind Tunnel. Model diameter = 0.62 m (2.04 ft).

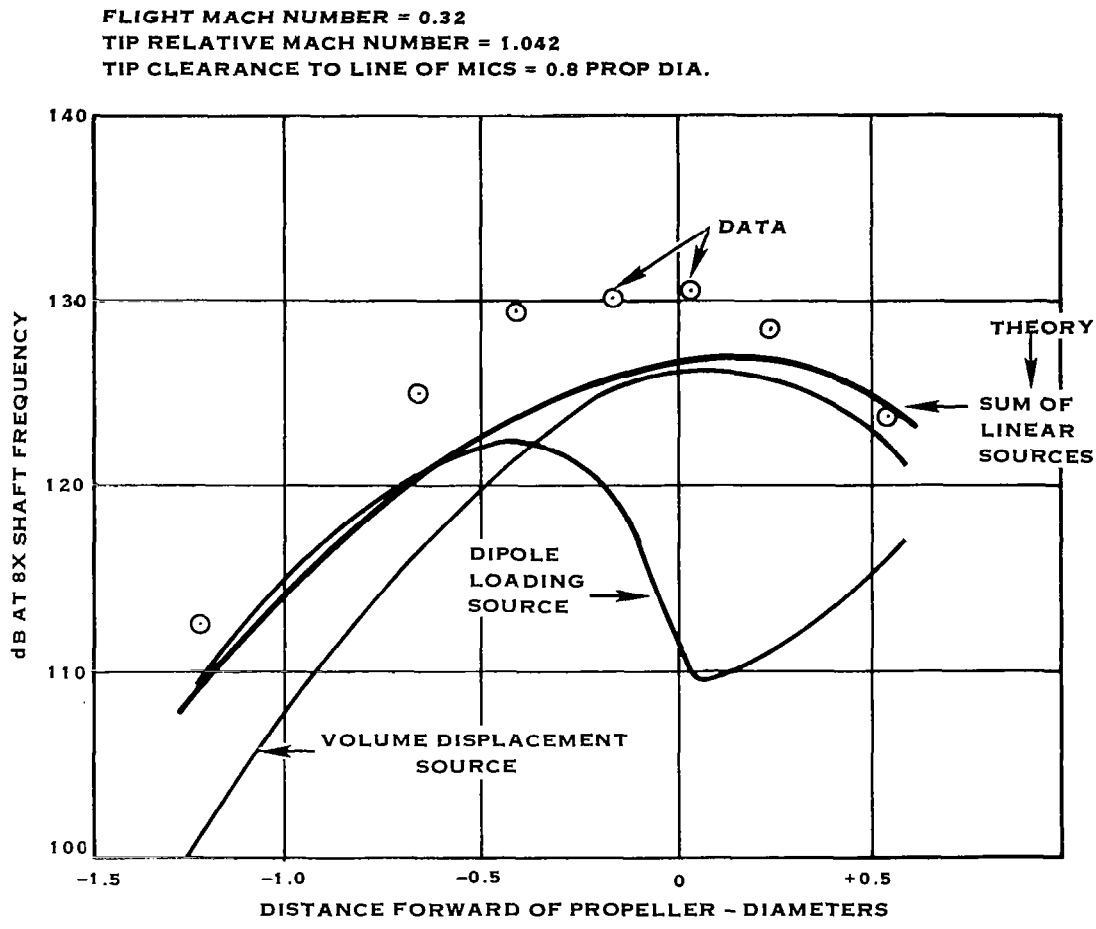

Figure 2.- Comparison of data with noise predicted for linear sources data from model shown in figure 1 tested with 2 blades. (Data corrected with Amiet's theory for tunnel shear layer refraction, ref. 18.)

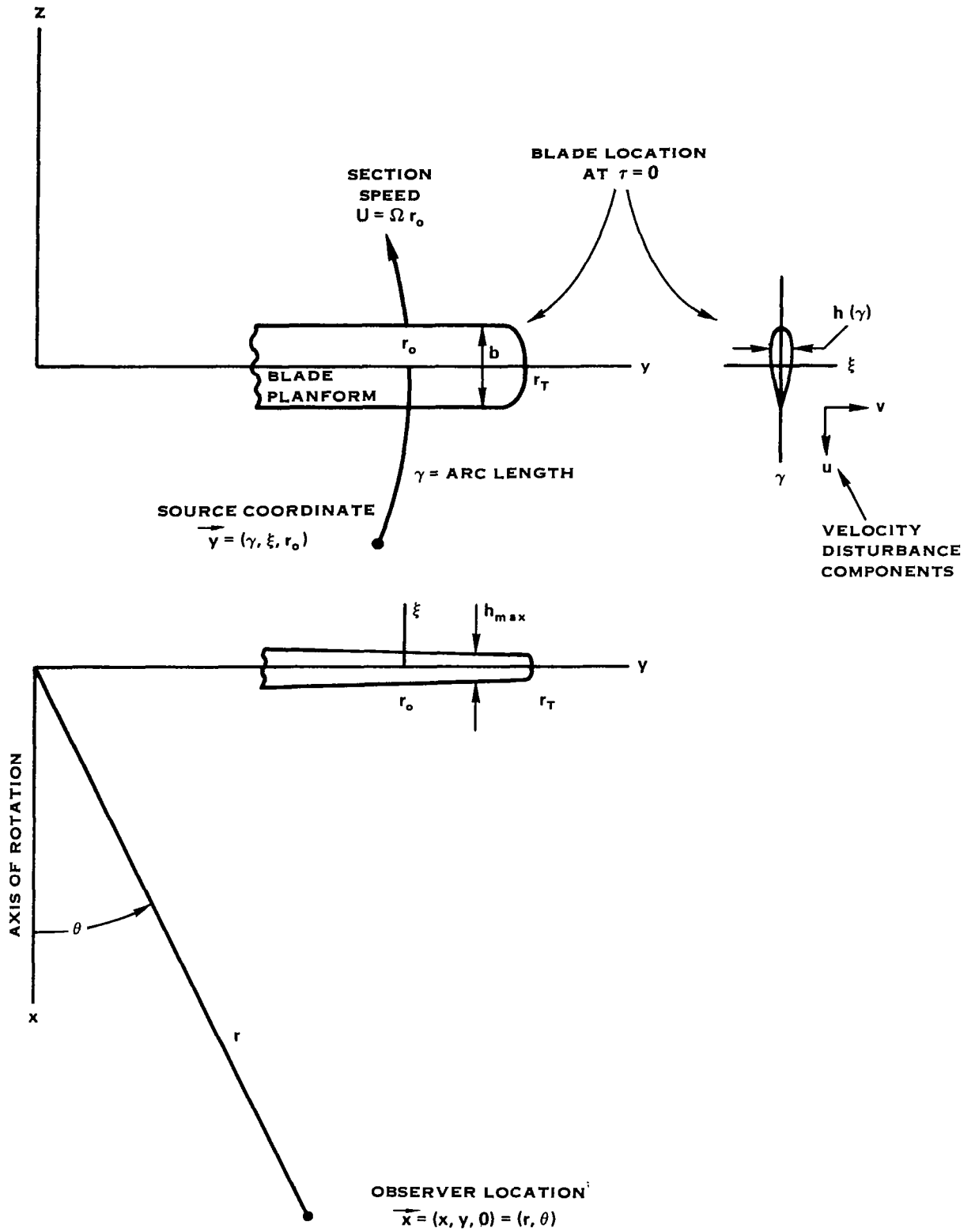

Figure 3.- Source and observer coordinates.

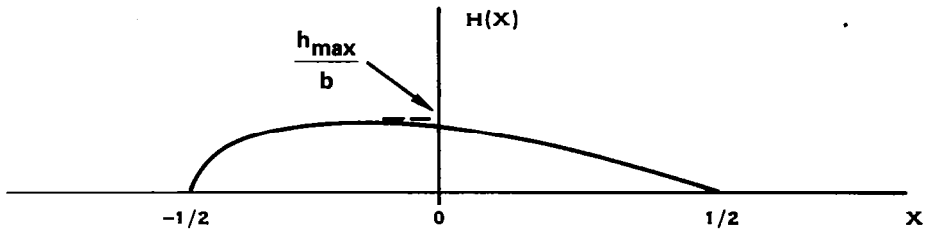

Figure 4.- Normalized airfoil thickness function.

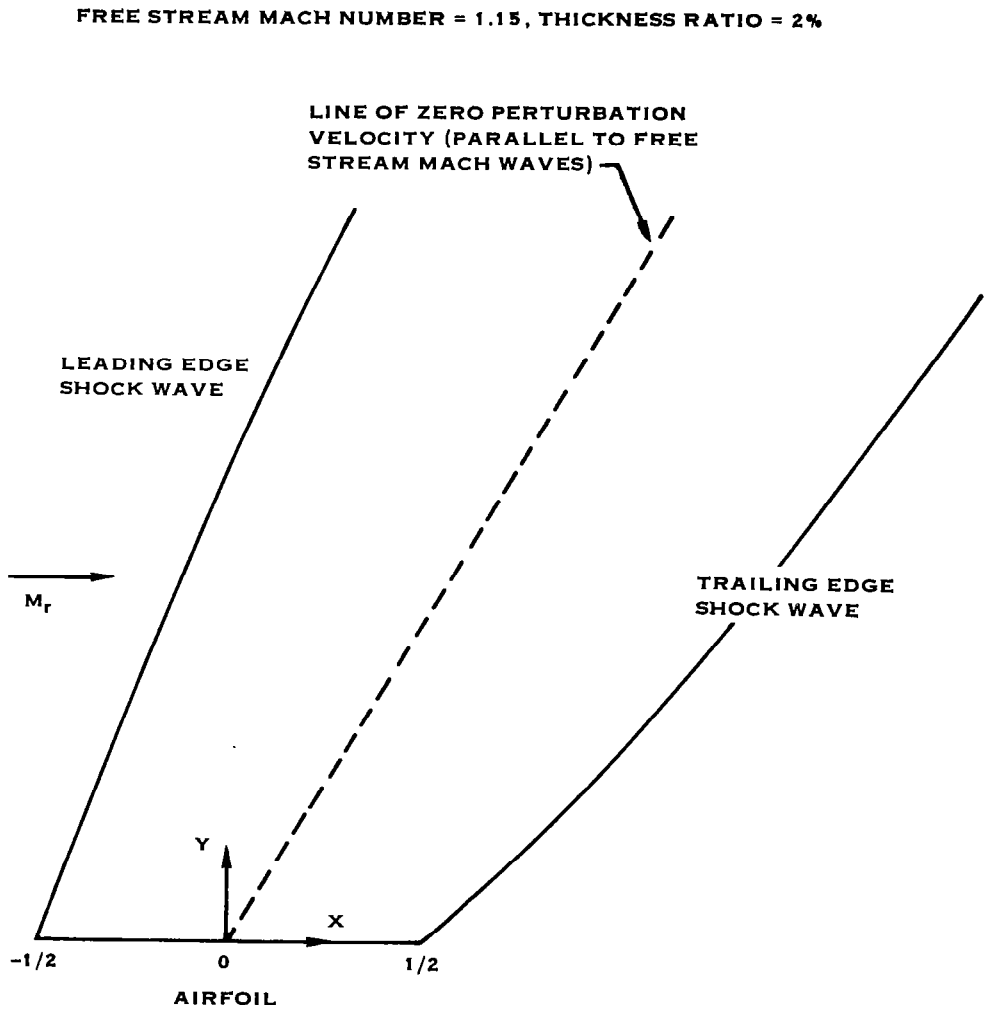

Figure 5.- Calculated shock wave pattern for parabolic arc airfoil in fully supersonic flow.

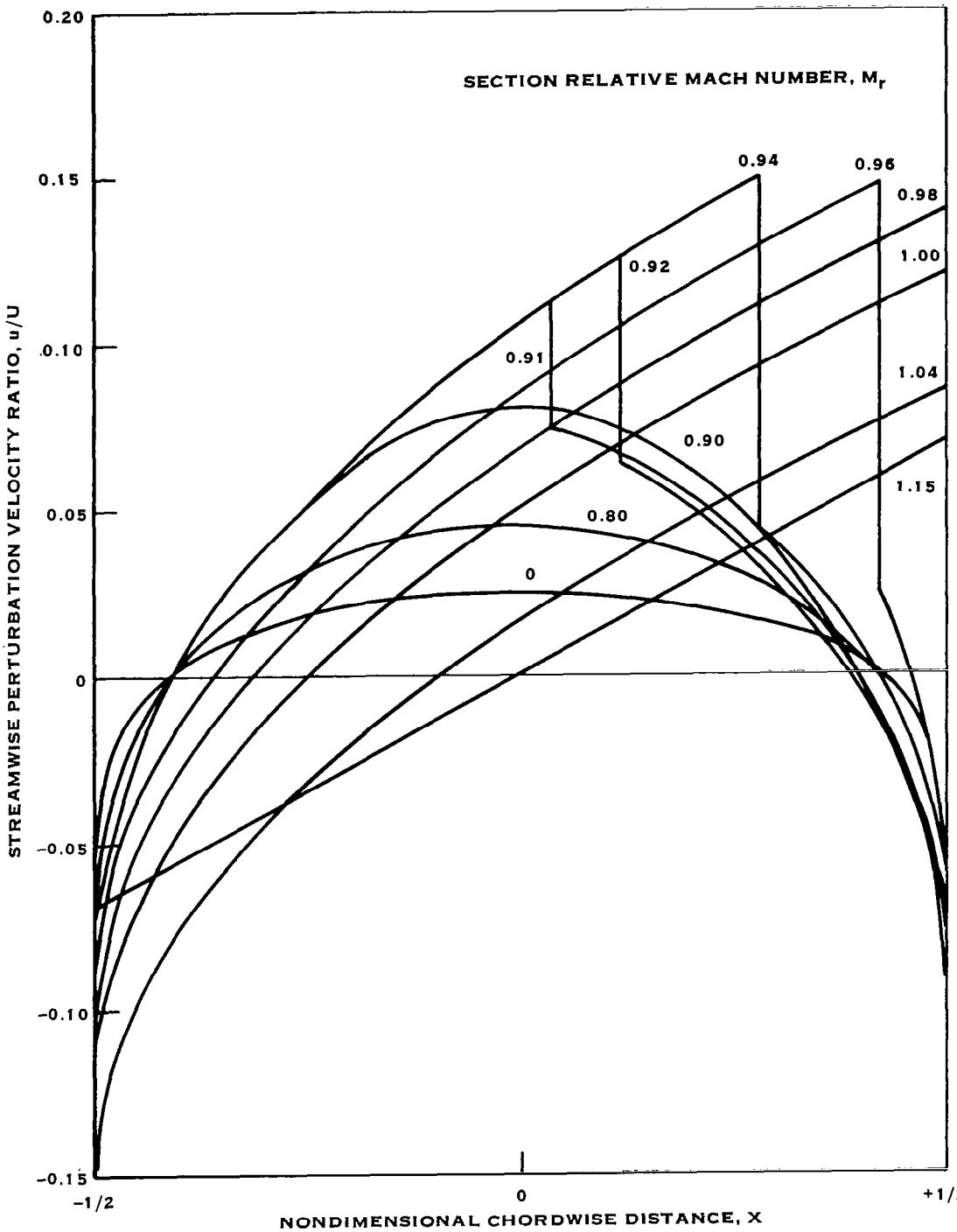

Figure 6.- Calculated chordwise velocity distributions for 2% thickness ratio parabolic arc airfoil.

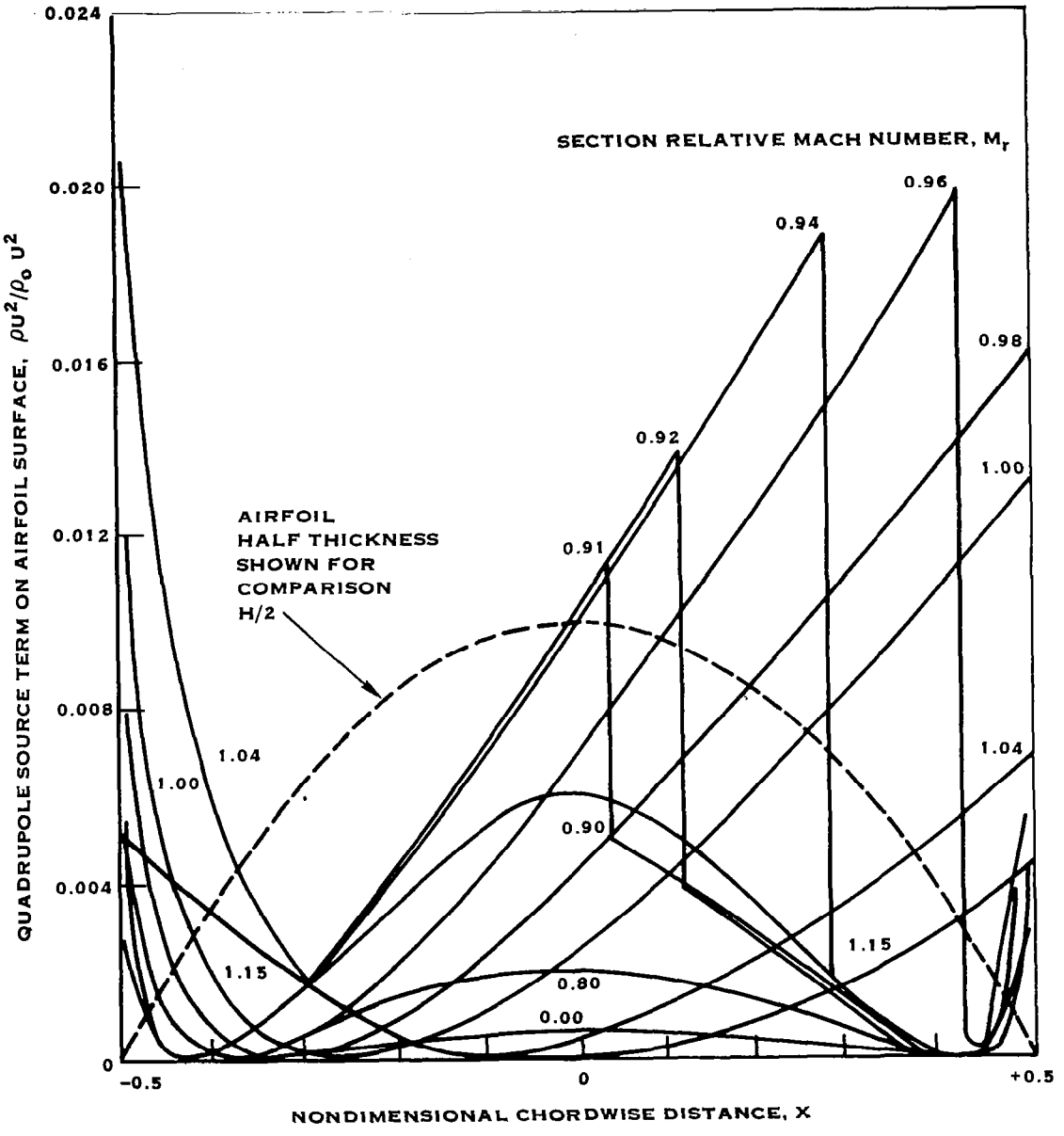

Figure 7.- Calculated quadrupole source strength along the surface of a 2% thickness ratio parabolic arc airfoil at transonic speeds.

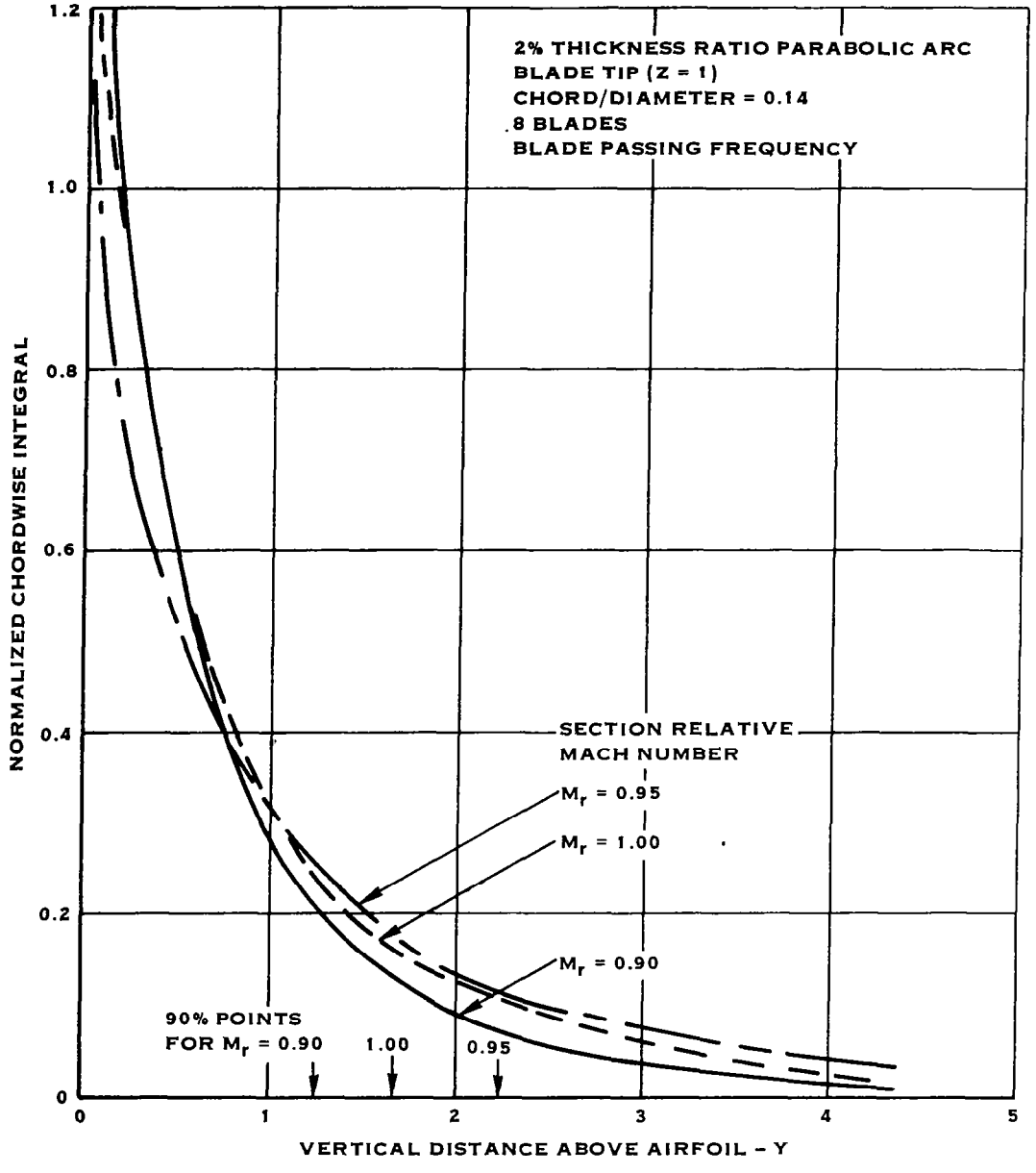

Figure 8.- Vertical distribution of quadrupole source strength. 90% points indicate value of Y which includes 90% of the quadrupole integral.

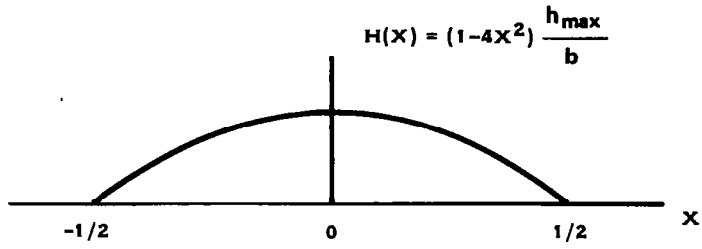

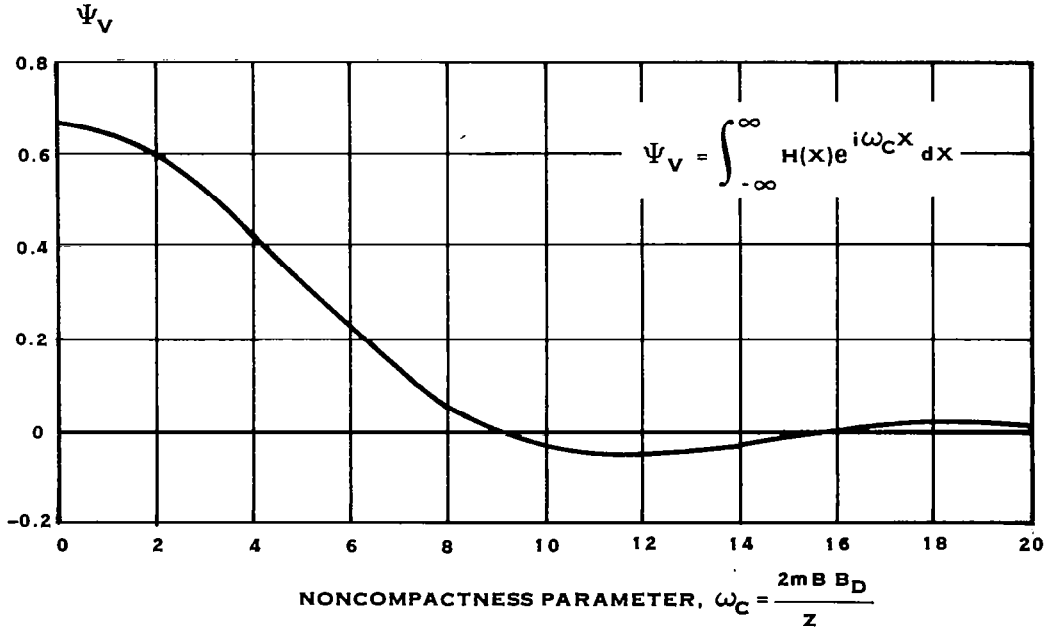

Figure 9.- Parabolic arc thickness distribution H(X) and its frequency domain counterpart Ψ_V.

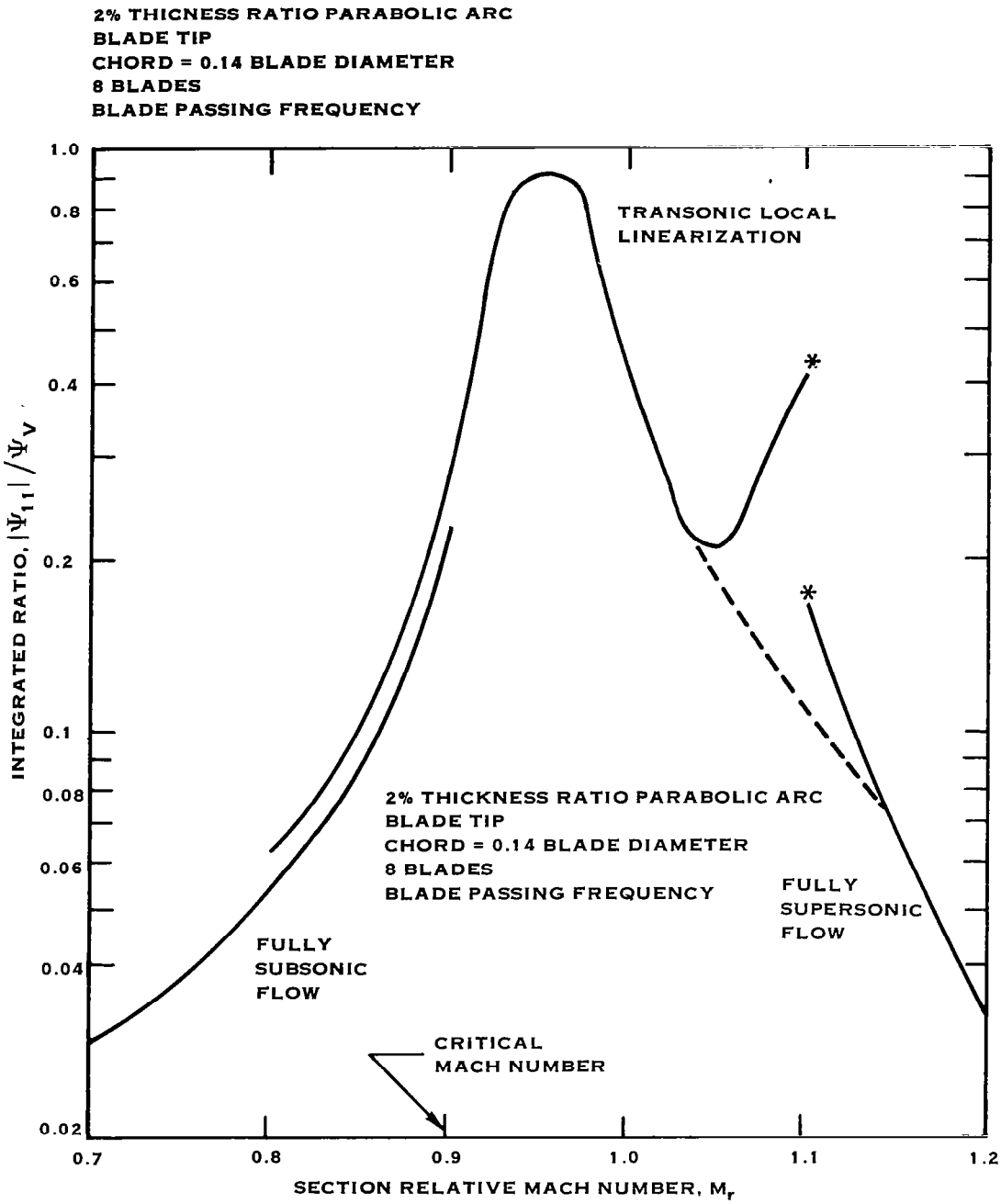

Figure 10.- Calculated ratio of integrated quadrupole strength $|\Psi_{11}|$ to integrated surface source strength Ψ_V. (Theory breaks down in regions denoted by *.)

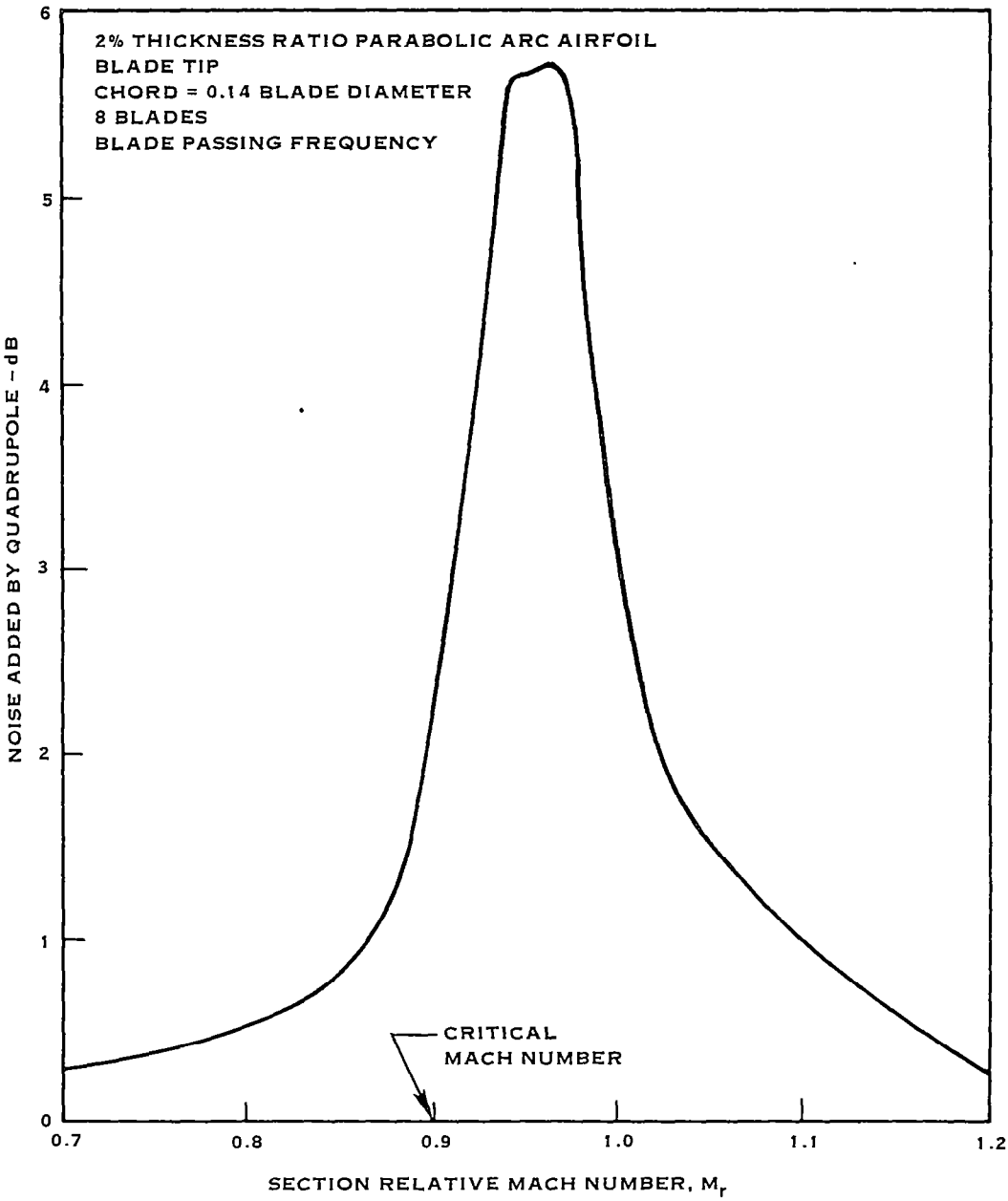

Figure 11.- Increase of blade thickness sound pressure level caused by including quadrupole noise.

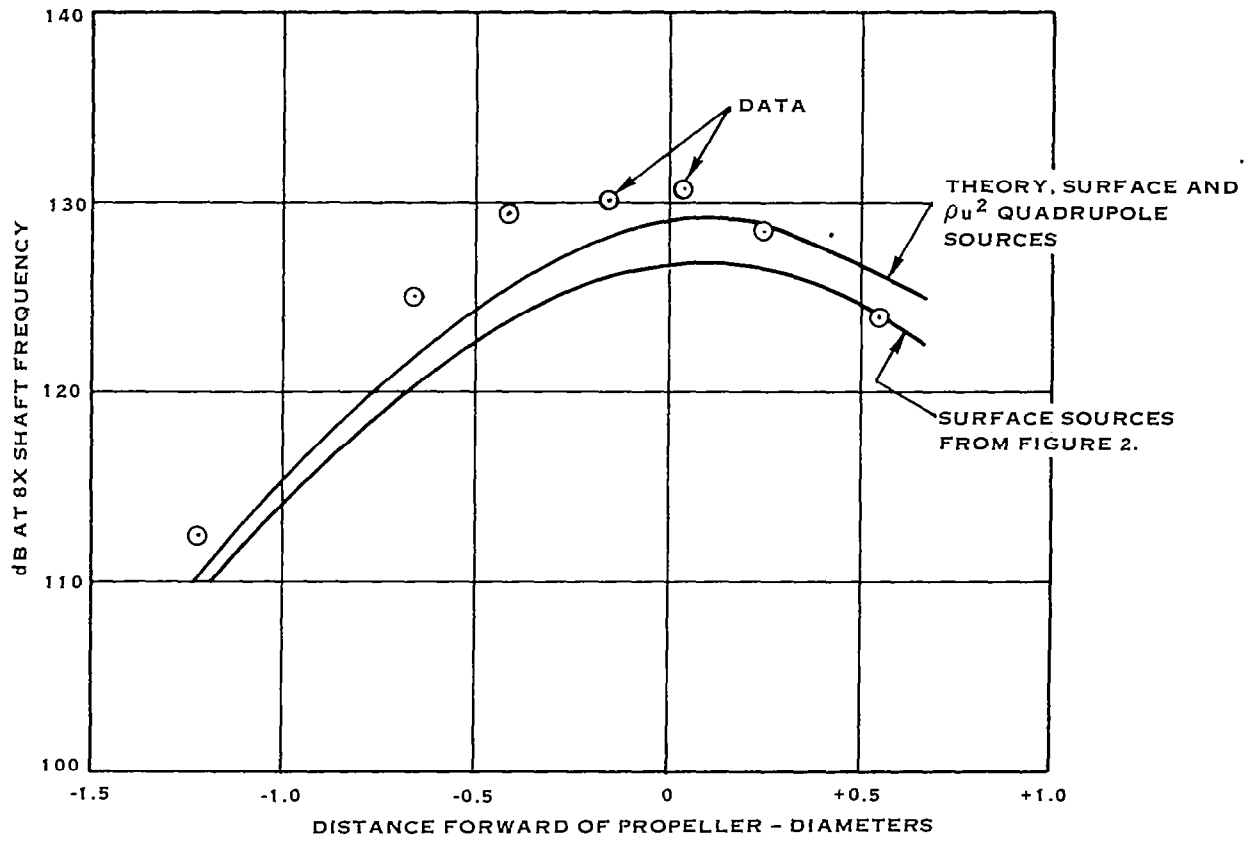

Figure 12.- Increase in noise caused by ρu^2 quadrupole and comparison with data. Same test conditions as figure 2.

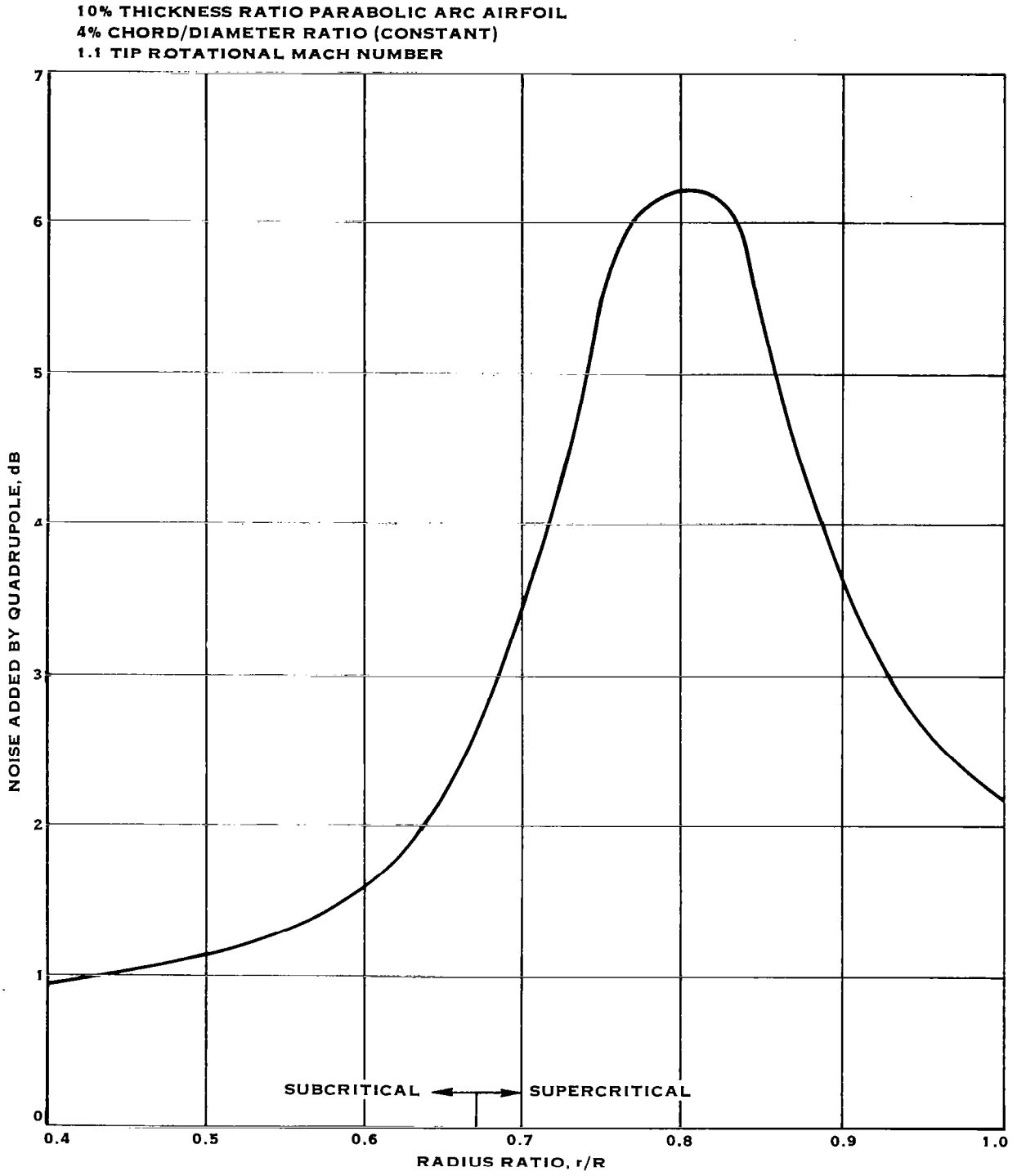

Figure 13.- Radial distribution of the quadrupole source on a helicopter blade.